Arch. Metall. Mater. **64** (2019), 3, 983-990

DOI: 10.24425/amm.2019.129484

I. DOBOSZ*#, W. GUMOWSKA*, M. CZAPKIEWICZ**

SYNTHESIS AND MAGNETIC PROPERTIES OF Fe NANOWIRE ARRAYS ELECTRODEPOSITED IN SELF-ORDERED ALUMINA MEMBRANE

Magnetic properties of Fe nanowire arrays (NWs) electrodeposited in anodic alumina membranes have been studied. The influence of nanowire geometry (length, pore diameter) and an external magnetic field applied during electrodeposition process on the magnetic properties of nanowire arrays was investigated. With the use of the X-ray diffraction analysis the structure of iron wires was determined. The iron wires have the regular Body Centered Cubic structure. Magnetic measurements show that shape anisotropy aligns the preferential magnetization axis along the wire axis. It was found that the application of an external magnetic field in a parallel direction to the sample surface induces magnetic anisotropy with an easy axis of magnetization following the nanowire axis. The dependence of the height of Fe wires on the electrodeposition time was determined.

Keywords: Anodic alumina membrane, hysteresis loop, iron, nanowires

1. Introduction

Nowadays, iron nanoengineering is a quickly developing branch of science and nanotechnology due to the possibility of the numerous amount of applications [1]. But at the same time their rapid development delivers more and more questions which are new or are still unclear and need to be commented. Despite the fact that in recent years plenty of publications have appeared showing how to manufacture iron-based nanostructures of different shapes the forms of one dimensional nanostructures are the most interesting from scientific and application points of view [2].

Nanostructured magnetic materials are used not only in the informatics technology and for the storage of electronic data [3-5] but also in many other domains such as medicine [6], automotive industry [7], environmental protection engineering, sensor [8-9] and catalysis technology.

Membrane parameters, electrodeposition parameters, selection of a metal as well as membrane preparation strongly affect the nanowire properties. Many studies have been performed to determine the magnetic properties of metal nanowires [10-12]. The study shown both an increase [13,14] and reduction [15,16] of coercivity value with decrease of nanowire diameter and length occurred with easy axis of magnetization along nanowires. Membrane parameters can also affect crystalline structure of nanowires [17]. Some studies show that the electrodeposition parameters such as electrolyte composition, temperature, pH or cathodic potential influence the structure and magnetic properties of nanowires [18-20]. The concentration of metal ions, external magnetic field applied during deposition as well as addition of buffering factor can have a favorable effect on the magnetic properties on the nanowires [18,21,22].

Magnetic properties of nanowires can be modify, among other, by the selection of a metal or alloy. The high a saturation magnetization (M_s), such as for Fe (1751 kA/m) and for CoFe (1910 kA/m) can achieve a high enough shape anisotropy [23]. The iron exhibits low cubic magnetocrystaline anisotropy. Therefore, an appropriate selection of the geometry of iron wires allows to improve the magnetic anisotropy. Some studies show that the magnetic squareness of iron nanowires with (200) orientation was larger than that with (110) orientation [24]. The total anisotropy represents the competition among magnetocrystaline, shape and magnetoelastic anisotropies and dipolar interaction [25]. Magnetoelastic anisotropy, originating from external stress on the ferromagnetic material, may also effect the direction of favored magnetization. The low porosity value and high misalignment of nanowires reduce dipolar interaction between nanowires which also strongly influence the magnetic properties [13].

Both the growth rate as well as the microstructure has been significantly improved with deposition in the external magnetic field. Relatively few studies have been carried out to investigate the influence of the magnetic field on the magnetic properties of a ferromagnetic metals deposited on the porous membrane surface [22,26-28]. The known phenomenon occurring with the application of the external magnetic field during the metal

* AGH, UNIVESITY OF SCIENCE AND TECHNOLOGY, FACULTY OF NON-FERROUS METALS, AL. MICKIEWICZA30, 30-059 KRAKOW, POLAND
** AGH, UNIVESITY OF SCIENCE AND TECHNOLOGY, FACULTY OF COMPUTER SCIENCE, ELECTRONICS AND TELECOMUNICATIONS, AL. MICKIEWICZA30, 30-059 KRAKOW, POLAND
# Corresponding author: iwona.dobosz@agh.edu.pl

electrodeposition is the magnetocrystalline effect. The magnetocrystalline effect consists in the change of the structure when an external magnetic field is applied.

Fe nanowires exhibit high magnetic coercivity resulting from the shape anisotropy and orientation of nanowire assemblies, nonetheless only a few publications have reported the morphology of Fe nanowires [23,29,30]. We examined which conditions, such as nanowire geometry and external magnetic field, are required to come close to the improvement of magnetic properties. An external magnetic field has been applied during the deposition in order to betterment an anisotropy along the direction of the nanowire growth. Improvement in the loop squareness is expected.

2. Experimental

The aluminum composition and the detailed information about the preparation of samples for the anodic oxidation process have been presented in the previous paper [22]. The anodic oxidation was carried out in two stages. The anodic alumina was formed at a constant voltage in the two solutions: 0.3 M oxalic acid at 2°C; 0.17 M phosphoric acid (V) at (–1) °C. The time of the first anodizing for oxalic acid solutions was 24 hours, whereas for the orthophosphoric acid – 2 hours. After the first anodizing stage, the oxide film was removed by immersing the samples into the solution of the composition: 0.6 M H_3PO_4; 0.2 M CrO_3, at 80°C for 2 hours. After removal of the oxide film, the samples were subjected to the second anodizing stage under the same conditions as the first one. The time of the anodizing process affects the thickness of the oxide films. The second anodizing process for the solutions of oxalic, and orthophosphoric acids lasted for 6, and 10 hours, respectively. After two anodizing stages, the aluminum substrate was removed in the mixture of the 0.2 M HCl and 0.1 M $CuCl_2$ solution in order to open pores. The barrier layer on the sample bottom was etched in 0.86 M H_3PO_4 at 30°C. After removal of both the aluminum and the barrier layer, a thin film of gold was sputtered onto the sample surface from the side of the open pores in order to provide an electric contact during the process of the electrodeposition of nanowires. In the areas from which the aluminum substrate was removed, a film of cooper was deposited by means of electrolysis in potentiostatic conditions. The diagram of the electrolyzer used in the experiment and the methodology of the preparation of the membrane is provided in detail in the paper [23].

The alumina membranes of nanoporous and ordered structure with defined pore dimensions (diameter, height, distance between them) were obtained. During the electrolysis process, the Fe was deposited cathodically in the pores of the obtained membranes. The process carried out in sulfate solutions with composition of: 0.5 M $FeSO_4$; 0.3 M H_3BO_3; 0.25 M $C_6H_8O_6$. The pH value of the solution was 3 and it was controlled by adding sulfuric acid (VI) or sodium hydroxide. All experiments were carried out at the room temperature (24°C) in the three-electrode system, where as a reference electrode a saturated calomel electrode was used (SCE, 0,241 V vs. SHE). All the potentials were recorded in relation to the SCE electrode, and then converted and presented with reference to the standard hydrogen electrode (SHE). A platinum plate used as the counter electrode. The area of the working electrode surface was 0.785 cm^2. The experiment was carried out with "IPS AJ" potentiostat. The potential was selected on the basis of the chronoamperometric and cycling voltamperometry experiments, and it was –0.8 V (vs. SHE). Finally, as a shown in Fig. 1 the Fe nanowire arrays were prepared by deposition into alumina membrane.

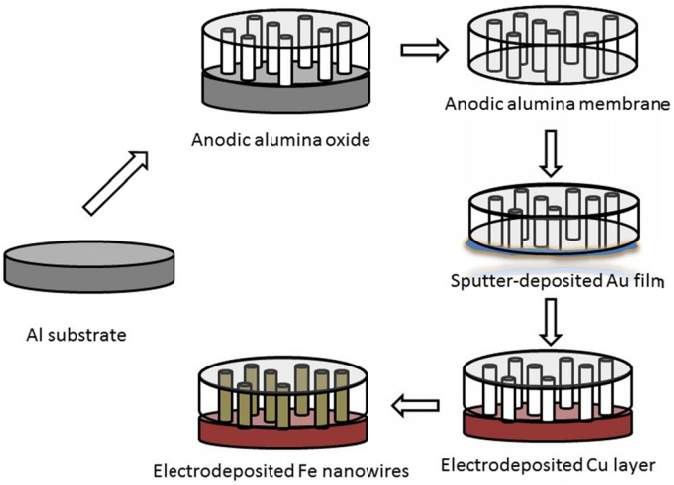

Fig. 1. The synthesis process of iron nanowire arrays scheme

During the process of the cathodic deposition of Fe nanowires in the magnetic field, the HV7 Walker Scientific electromagnet was used. The experiment was conducted in a homogenous external magnetic field of up to 0.7 T parallel or perpendicular to the electrode surface. The morphology of the oxide films and their cross-sections were observed with the use of the high resolution scanning electron microscopy with the field emission. The scanning microscope (HITACHI S-4700°) was equipped with an EDS system for the chemical composition analysis (NORAN VANTAGE). Structural studies was carried out with the use of the X-ray diffractometer (BRUKER AXS "Discover 8") with filtered $Cu_{K\alpha}$ radiation. The investigation of the magnetic hysteresis loop and its parameters (coercivity, saturation field, saturation magnetization and the remanence) was conducted with the use of the Resonance Vibrating Sample Magnetometer (R-VSM) in the magnetic field directed both perpendicular and parallel to the wire axis.

3. Results

3.1. Structural and morphological properties of Fe nanowires

The electrodeposition of Fe nanowire arrays was carried out in the membrane pores of the following dimensions: the diameter of the pores D_p = 70 nm, the distance between the

pores D_c = 110 nm. During the electrodeposition process, different electrolysis times were applied: 90, 300, 600, 1800, and 2100 seconds. The potential was kept constant and it was equal –1.0 V (vs. SHE). The relationship between the length (L) of iron wires and electrodeposition time is shown in Table 1.

TABLE 1

The dependence of the iron nanowires length on potentiostatic deposition time

Time, [s]	Length (L), [μm]
90	2,0±0,1
300	3±0,2
600	4±0,5
1800	8,7±0,6
2100	10±0,4

Fig. 2 shows an exemplary photo of cross- section the Fe nanowire arrays deposited in the pores of the Al_2O_3 membrane (the length of the nanowires $L \approx 3$ μm). The nanowires are built in uniformly and their length, under constant electrodeposition potential, depends on the process time. The SEM investigation shows that the formation of wires starts in the lower part of the Al_2O_3 membrane from the Cu layer.

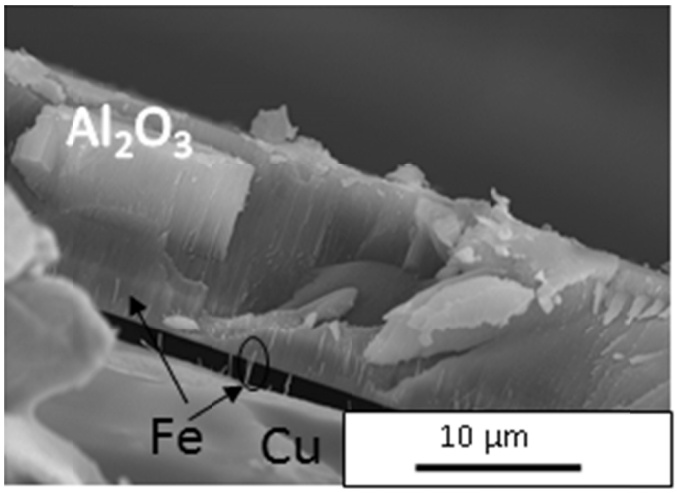

Fig. 2. A cross-sectional SEM image of the Fe NWs deposited in the pores of membrane with the dimensions: D_p = 70 nm, D_c = 110 nm under potential –1.0 V (vs. SHE). The time of electrodeposition: 300 seconds. The length of the wires was about 3 μm

The X-ray diffraction pattern is presented in Fig 3. In the diffraction pattern, clear reflections characteristic for the Fe of the crystallographic indices (110), (200), (211), and (310) can be seen. On the basis of the X-ray analysis it was found that the iron wires of the BCC structure had been built in the pores of the alumina membrane.

Hu et al. found that the magnetic squareness of Fe nanowires with (200) orientation was larger than that with (110) orientation [25]. Our study demonstrate stronger peak at 2θ = 65.5° corresponding to the (200) plane which is attributed to the easy direction of magnetization. However, Neetzel et al. show that

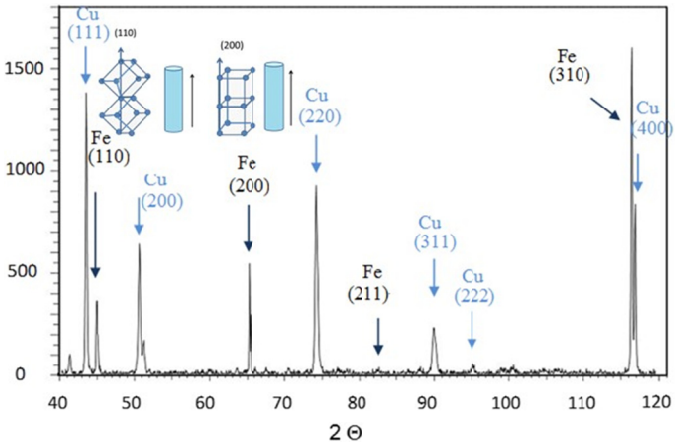

Fig. 3. XRD patterns for the iron nanowire arrays with diameter of 70 nm and length of 3 μm obtained under potential –1.0 V (vs. SHE). The peaks characteristic for the iron and cooper are described with the indices of crystallographic planes

potentiostatic deposition (–1.0 V vs. SHE) led to a preferred (110) orientation [24].

3.2. Magnetic properties of Fe nanowires

3.2.1. The effect of nanowire geometry

The magnetic properties of the iron NWs deposited at different potentials were investigated in the magnetic field directed both perpendicular and parallel to the wire axis with the use of the R-VSM vibration magnetometer. The hysteresis loops are presented as the relationship between the magnetization to saturation magnetization ratio (M/M_s) and the magnetic field strength (H).

To perform an analysis of the relationship between the magnetization and the magnetic field strength, the following values have been determined or defined: magnetic field strength (H), magnetization (M), coercive field (H_c), M_r/M_s remanence squareness, where M_r – residual magnetization (remanence), M_s – saturation magnetization, remanence energy $\mu_0 M_r H_c \cdot V$, where V is nanowires volume.

The effect of the length of the wire (range 3 ¸ 10 μm) on the shape of hysteresis loop is shown in Fig. 4a-d for nanowires with a 70 nm pore diameter and in Fig. 4e for nanowires with 100 nm pore diameter. The values characterizing the magnetic properties of the iron NWs are presented in Table 2.

For the shorter wires with the length of 3 and 4 μm (Fig. 4a,b) the hysteresis loops measured parallel and perpendicular to the wire axis almost coincide. These measurements show isotropic magnetic behavior. Once a sufficient wire length occurs (9 μm), the magnetic anisotropy reveals and an increase of coercive field (from 246 Oe to 331 Oe) is observed. The magnetic measurements show that the easy axis of magnetization is oriented parallel to the long wire axis in agreement with previous results [30,31]. The longest wires of 10 μm (Fig. 4d)

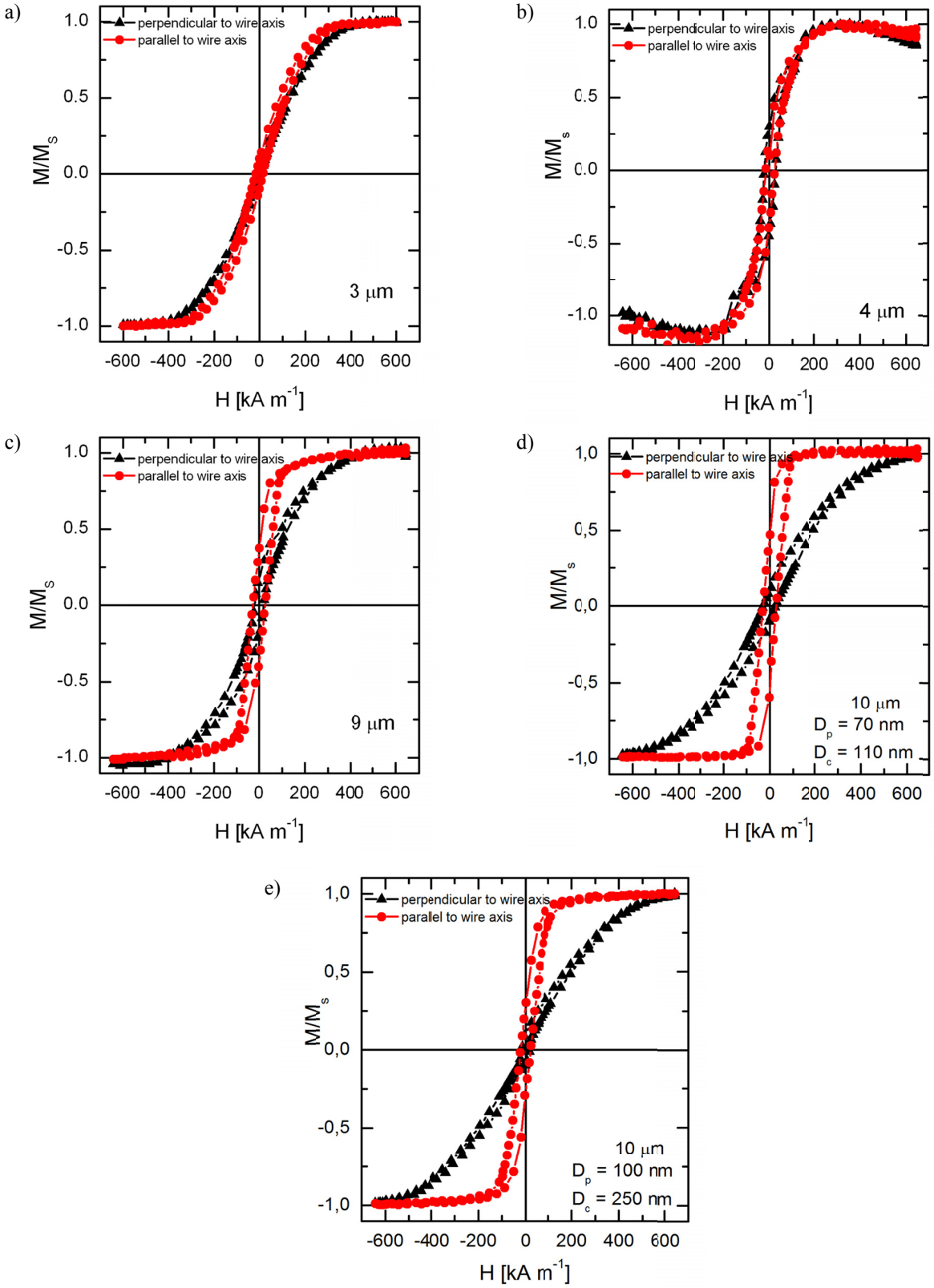

Fig. 4. The hysteresis loops of the iron NWs with diameters of 70 nm obtained in the process of the electrodeposition for different times: a) 300, b) 600, c) 1800, d) 2100 seconds and e) nanowires with diameter of 100 nm. Electrodeposition was conducted under potential –1,0 V

demonstrate a clearly visible privileged magnetization direction along the axis of wires (easy direction), whereas the field direction perpendicular to the axis of wires is the difficult direction. This is confirmed by visible differences in values of remanence energy and squareness M_r/M_s calculated for parallel and perpendicular geometry curves (Table 2). We obtained the largest value of coercive field (344 Oe) for the nanowires with the 70 nm of diameter and 10 μm of length while smaller coercivity (283 Oe) and squareness were observed for the nanowires with the same length but larger diameter of 100 nm.

TABLE 2

The values characterizing the magnetic properties of the iron NWs of different length (L) and pore diameter (D_p)

L [μm]	D_p ; D_c [nm]	Remanence energy $\mu_0 M_r \cdot H_c \cdot V$ [J]		Squareness M_r/M_s		Remanence M_r [emu/cm^3]		Coercivity H_c [kA/m]	
		(II) $\times 10^{-16}$	(⊥) $\times 10^{-16}$	(II)	(⊥)	(II)	(⊥)	(II)	(⊥)
		to wire axis							
3	70 ; 110	0,4 (0,25 keV)	0,07J (0,05 keV)	0,10	0,04	168	71	16,5 (206 Oe)	7,3 (91 Oe)
4		1,78 (1,11 keV)	2,82 (1,76 keV)	0,27	0,35	470	603	19,7 (246 Oe)	24,3 (304 Oe)
9		6,74 (4,2 keV)	2,51 (1,57 keV)	0,36	0,18	608	312	26,5 (331 Oe)	19,2 (240 Oe)
10		10,9 (6,8 keV)	2,22 (1,39 eV)	0,48	0,10	826	168	27,5 (344 Oe)	27,5 (344 Oe)
10	100 ; 250	10,9 (6,8 keV)	2,56 (1,6 keV)	0,29	0,1	462	194	22,6 (283 Oe)	15,9 (199 Oe)

In Fig. 5 we show the value of remanence normalized to saturation magnetization (M_r/M_s) measured with magnetic field applied along and perpendicular to the nanowire axis as a function of length. The largest differences of the squareness within the sample plane and perpendicularly to it is observed for the longest wires, i.e. 10 μm (Fig. 5). This demonstrates that the distribution of magnetization becomes close to isotropic for small lengths.

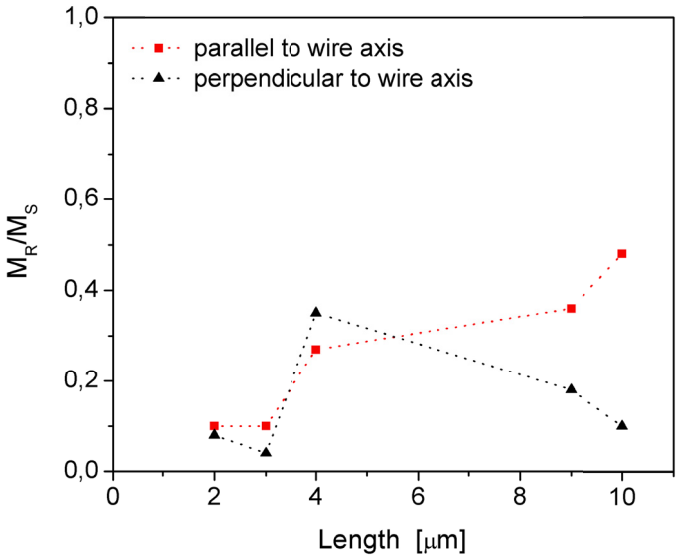

Fig. 5. The relationship between the squareness measured parallel and perpendicular to the wire axis as a function of the length of the Fe wires deposited in the membrane of the pore dimensions D_p = 70 nm, D_c = 110 nm

As shown above the length of Fe NWs significantly affects the magnetic properties. With the increase of the nanowire length the shape anisotropy increase (Fig. 5). For longer wires the easy magnetization direction is oriented along the wire axis. To understand the present results, it is necessary to consider multipolar interactions between wires. Multipole interactions between the nanowires can also strongly influence the magnetic properties.

The simplest description of the interaction of two nanowires comes down to the determination of the demagnetization field (H_z) generated by one of the wires located at the D_c distance from the second one. In accordance with the Kumar's [32] and Sorop's [33] studies, the demagnetization field can be described with the formula Eq. (1):

$$H_z = -\frac{m}{\sqrt[3]{D_c^2 + \frac{L^2}{4}}} \tag{1}$$

where m is the dipole moment ($m = M_s V$), and the V – wire volume.

On the basis of Equation (1) the $H_z = f(L)$ graph has been made (Fig. 6). The graph illustrating the relationship between the demagnetization field and the wire lengths results from a model of the magnetostatic interaction between wires and it can be used for the estimation of the interaction influence only.

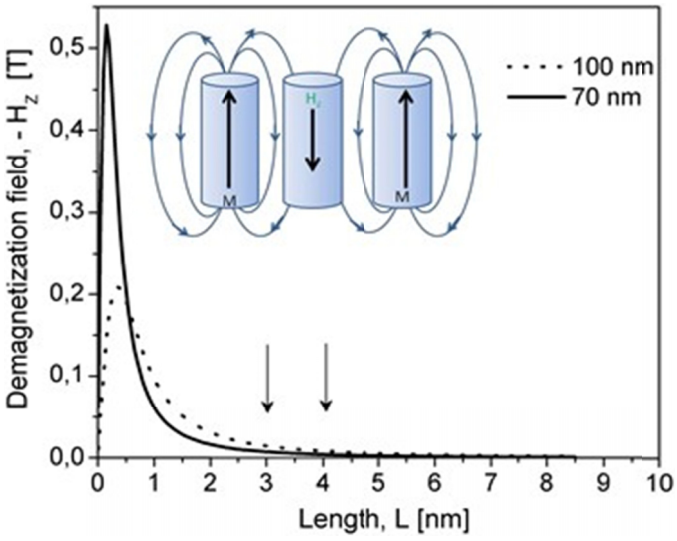

Fig. 6. The influence of the Fe nanowire length on the demagnetization field – H_z (D_p = 70 nm and 100 nm)

In addition, the H_z value is dependent not only on the length (L) of nanowires, but also on the pore diameters (D_p) and the distance between pores (D_c).

This relationship has its maximum which corresponds to the highest H_z value in connection with wire lengths. The maximum value occurs for the wires of the lengths below 1 μm. The demagnetization field (H_z) is formed as the result of the interaction of nanowires and it forces the magnetization (M) of the opposite orientation. Therefore, the lower the demagnetization field is, the higher is the magnetization. Thus, the Fe wire arrays of the length 9 and 10 μm (D_p = 70 nm) show the highest magnetization value. This result is similar to other reports [33].

As is well know the magnetic behavior of the nanowires is mainly a result of the competition between shape anisotropy, magnetocrystaline anisotropy, magnetoelastic anisotropy and dipolar interaction between wires [10]. Magnetoelastic anisotropy originating from external stress on the ferromagnetic material, may also affect the direction of favored magnetization. The X-ray phase analysis (Fig. 3) indicates that the structure of Fe wires is of the body-centered cubic (BCC) for which the magnetocrystalline anisotropy is small. It is in agreement with the work of [34,35]. This means that the magnetization direction depends mainly on the shape anisotropy and dipolar interaction between the nanowires, therefore on the length and the diameter of wires as well as the distance between them. When the length of the wires is long-range the shape anisotropy favors the magnetization direction along the nanowires. Whereas when the length of the wires is restricted then the demagnetization factors depends on the aspect ratio and it can change the direction of magnetization to perpendicular to the wire axis. Our measurements indicate that for the nanowires with the length of above 9 nm the easy axis is along the wire, while for shorter it gradually loses the defined orientation. Besides, for the Fe nanowires, the anisotropy energy along the nanowire axis is sufficiently high (in comparison with the coupling energy between neighboring wires) to provide domination of the easy direction along the wire axis within the investigated length range.

3.2.2. The effect of external magnetic field

In the process of the electrodeposition of iron, the magnetic field (0.7 T) directed perpendicularly (⊥) and parallel (||) to the

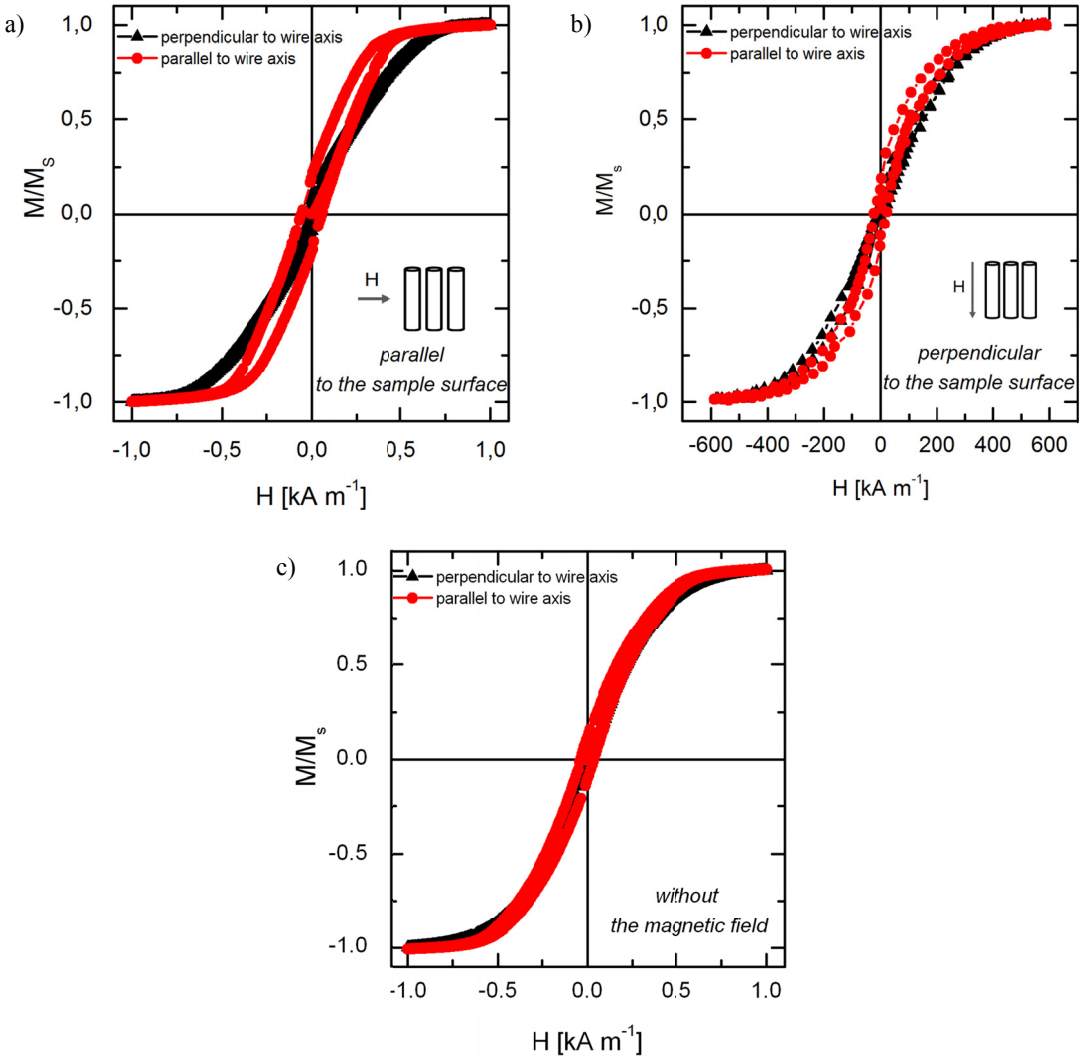

Fig. 7. The hysteresis loops for the Fe NWs obtained under potential –1,0 V; a) in an external magnetic field 0.7 T – parallel to the sample surface, b) in an external magnetic field 0.7 T – perpendicular to the sample surface, c) without magnetic field

TABLE 3

The values characterizing the magnetic properties of the Fe nanowires obtained without and with external magnetic field (0.7 T) applied perpendicularly and parallelly to the membrane surface. The length of the nanowires L = 2 μm

Configuration	Remanence energy $\mu_0 M_r \cdot H_c \cdot V$ [J]		Squareness M_r/M_s		Remanence M_r [emu/cm^3]		Coercivity H_c [kA/m]	
	(II) $\times 10^{-16}$	(⊥) $\times 10^{-16}$	(II)	(⊥)	(II)	(⊥)	(II)	(⊥)
	to wire axis							
0T	0,51 (0,32 keV)	0,26 (0,16 keV)	0,10	0,08	180	142	29,6 (370 Oe)	19,2 (240 Oe)
0,7T ∥	1,45 (0,9 keV)	0,23 (0,15 ke)V	0,19	0,09	331	161	45,6 (570 Oe)	15,2 (190 Oe)
0,7T ⊥	0,49 (0,31 keV)	0,11 (0,07 keV)	0,13	0,05	223	80	22,9 (286 Oe)	13,9 (174 Oe)

sample surface was applied. An Al_2O_3 membrane with the pores diameter 70 nm distanced by 110 nm was used. In order to examine the influence of the external magnetic field on magnetic properties and to exclude the influence of the shape geometry of Fe wires, samples with a similar wire length of approx. 2 μm were selected. Hysteresis loops are shown in Fig. 7 and magnetic parameters are collected in Table 3.

The Fe nanowire arrays deposited with external magnetic field parallel to the sample surface demonstrate a slight magnetic anisotropy with easy axis of magnetization along nanowire axis. For the wires deposited without magnetic field and in external magnetic field of 0.7 T in the configuration perpendicular to the membrane surface magnetization becomes isotropic or close to isotropic, respectively. This results is similar to other reports [28].

The application of the external magnetic field of 0.7 T in the configuration parallel to the membrane surface (i.e. perpendiculary to the wire axis) (Fig. 7a) slightly affects the changes in magnetic properties. This behavior may be due to the fact that iron grains in a zero magnetic field may have random orientations and the effect of a magnetic field may cause a magnetic ordering that increases the anisotropy [21,26].

4. Conclusions

We investigated Fe nanowire arrays with different geometry prepared into anodic alumina membranes with external magnetic field applied during electrodeposition process. The diffraction analysis of iron nanowires indicates the presence of the Fe phase of the Body Centered Cubic (BCC) lattice with a strong reflection originated from the phase (110) and (200). The SEM images of the cross-section revealed nanowires embedded into pores of alumina membrane. The measurements showed that an impact of nanowire geometry on the magnetic parameters is great. The performed studies allowed us to determine the dimensions of wires optimal for obtaining Fe nanowires with the beneficial magnetic characteristics. The application of the external magnetic field in the direction parallel to the sample surface during the process of the cathodic reduction of Fe^{2+} ions induce an anisotropy with an easy axis along the direction of the nanowire growth. We find that long nanowires (approx. 10 μm) and small diameter are optimal to obtain nanowires with magnetic anisotropy with an easy axis along the nanowire and high coercivity value.

Acknowledgements

Authors wish to acknowledge Polish National Science Center [grant number UMO-2016/23/G/ST5/04058] for financial support.

REFERENCES

[1] G.L. Hornyak, J.J. Moore, H.F. Tibbals, J. Dutta, Fundamentals of Nanotechnology, CRC Press (2009).
[2] I. Higler, W.A. Kaiser, Nanomed. **7**, 1443-1459 (2012).
[3] R. Sharif, S. Shamaila, M. Ma, L.D. Yao, R.C. Yu, X.F. Han, Y. Wang, M. Khaleeq-ur-Raman, J. Magn. Magn. Mater. **320** (8), 1512-1516 (2008).
[4] C. Kim, T. Loedding, S. Jang, H. Zeng, Z. Li, Y. Sui, D.J. Sellmyer, Appl. Phys. Lett. **91**, 172508 1-3 (2007).
[5] D.J. Sellmyer, H. Zheng, M. Yan, S. Sun, Y. Liu, Handbook of Advanced Magnetic Materials. IV: Properties and Application, (2006).
[6] A. Hultgren, M. Tanase, C.S. Chen, D.H. Reich, J. Appl. Phys. **93**, 7554-7556 (2003).
[7] Y. Cui, C.M. Lieber, Science **291**, 851-853 (2001).
[8] P.D. McGary, L. Tan, J. Zou, B.J.H. Stadlera, J. Appl. Phys. **99**, 08B310 1-6 (2006).
[9] M. Yun, N.V. Myung, R. P. Vasquez, J. Wang, H. Monbouquette, Proceedings of the SPIE **5220**, 37 (2003).
[10] M. Kac, A. Zarzycki, S. Kac , M. Kopec, M. Perzanowski, E.M. Dutkiewicz, K. Suchanek, A. Maximenko, M. Marszalek, Mater. Scienc Eng. B **211**, 75-84 (2016).
[11] M. Kroll, W.J. Blau, D. Grandjean, R.E. Benfield, F. Luis, P.M. Paulus, L.J. de Jongh, J. Magn. Magn. Mater. **249**, 241-245 (2002).

[12] D. Ciuculescu, F. Dumestre, M. Comesana-Hermo, B. Chaudret, M. Spasova, M. Farle, C. Amiens, Chem. Mater. **21**, 3987-3995 (2009).

[13] J. Rivas, A. Kazadi Mukenga Bantu, G. Zaragoza, M.C. Blanco, M.A. LopezQuintela, J. Magn. Magn. Mater. **249**, 220-227 (2002).

[14] Z. Ye, H. Liu, Z. Luo, H.-G. Lee, W. Wu, D.G. Naugle, I. Lyuksyutov, Nanotechn. **2**, 045704 1-8 (2009).

[15] Y. Ren, Q.F. Liu, S.L. Li, J.B. Wang, X.H. Han, J. Magn. Magn. Mater. **321**, 226-230 (2009).

[16] D. Kaur, S. Chaudhary, D.K. Pandya, J. Appl. Phys. **114**, 043909 1-5 (2013).

[17] A. Fert, L. Piraux, J. Magn. Magn. Mater. **200**, 338-351 (1999).

[18] C.X. Cui, B.L. Wang, W. Yang, J.B. Sun, J. Cryst. Growth **324** (1), 168-171 (2011).

[19] X. Han, Q. Liu, J. Wang, S. Li, Y. Ren, R. Liu, F. Li, J. Phys. D Appl. Phys. **42** 095005 (2009).

[20] F. Li, T. Wang, L. Ren, J. Sun, J. Phys. Condens. Matter. **16**, 8053-8060 (2004).

[21] H.R. Khan, K. Petrikowski, Materials Science Forum **373-376**, 725-728 (2001).

[22] S. Ge, Ch. Li, X. Ma, W. Li, L. Xi, C.X. Li, J. Appl. Phys. **90** (1), 509-511 (2001)

[23] V. Haehnel, S. Fahler, P. Schaaf, M. Miglierini, C. Mickel, L. Schultz, H. Schlorb, Acta Mater. **58**, 2330-2337 (2010).

[24] C. Neetzel, T. Ohgai, T. Yanai, M. Nakano, H. Fukunaga, Nanosc. Res. Lett. **12**, 598-605 (2017).

[25] H.N. Hu, H.Y. Chen, S.Y. Yu, J.L. Chen, G.H. Wu, F.B. Meng, J.P. Qu, Y.X. Li, H. Zhu, John Q. Xiao, J. Magn. Magn. Mater. **295**, 257-262 (2005).

[26] J. Sa´nchez-Barriga, M. Lucas, G. Rivero, P. Marin, A. Hernando, J. Magn. Magn. Mater. **312**, 99-106 (2007).

[27] H.R. Khan, K. Petrikowski, Mater. Sci. Eng. C **19**, 345-348 (2002).

[28] G. Han, J. Lu, Y. Gao, J. Magn. Magn. Mater. **393**, 199-203 (2015).

[29] D. Sellmyer, M. Zheng, R. Skomski, J. Phys.: Condens. Matter. **13**, R433-R460 (2001).

[30] P.M. Paulus, F. Luis, M. Kröll, G. Schmid, L.J. de Jongh, J. Magn. Magn. Mater. **224**, 180-196 (2001).

[31] S. Yang, H. Zhu, D. Yu, Z. Jin, S. Tang, Y. Du, J. Magn. Magn. Mater. **222**, 97-100 (2000).

[32] A. Kumar, S. Fähler, H. Schlörb, K. Leistner, L. Schultz, Phys. Rev. B **73**, 064421-5 (2006).

[33] T.G. Sorop, K. Nielsch, P. Goring, M. Kroll, W. Blau, R.B. Wehrspohn, U. Gosele, L.J.d. Jongh, J. Magn. Magn. Mater. **272-276**, 1656-1657 (2004).

[34] J. Wang, X. Zhou, Q. Liu, D. Xue, F.S. Li, B Li, Nanotechn. **15**, 485 (2004).

[35] G. Huang, Y. Xie, X. Wu, L.W. Yang, Y. Shi, G. Siu, J. Cryst. Growth **289**, 295-298 (2006).